The $H+D_2$ reaction: Quantum-state distributions at collision energies of 1.3 and 0.55 eV

Klaus-Dieter Rinnen, Dahv A. V. Kliner, and Richard N. Zare
Department of Chemistry, Stanford University, Stanford, California 94305

(Received 13 July 1989; accepted 8 August 1989)

We have studied the $H + D_2 \rightarrow HD + D$ reaction using thermal D_2 ($\sim$298 K) and translationally hot hydrogen atoms. Photolysis of HI at 266 nm generates H atoms with center-of-mass collision energies of 1.3 and 0.55 eV, both of which are above the classical reaction barrier of 0.42 eV. The rovibrational population distribution of the molecular product is measured by (2 + 1) resonance-enhanced multiphoton ionization (REMPI). The populations of all energetically accessible HD levels are measured. Specifically, we observe $HD(v = 0, J = 0\text{–}15)$, $HD(v = 1, J = 0\text{–}12)$, and $HD(v = 2, J = 0\text{–}8)$. Of the available energy, 73% is partitioned into product translation, 18% into HD rotation, and 9% into HD vibration. Both the rotational and vibrational distributions are in remarkably good agreement with quasiclassical trajectory (QCT) calculations, though the calculated rotational distributions are slightly too hot. We discuss factors contributing to the success of the QCT calculations.

I. INTRODUCTION

The reactions of translationally hot atoms have been the focus of experimental and theoretical studies for more than half a century.[1] In some of the earliest hot H-atom experiments, the atoms were generated by nuclear recoil,[2-4] i.e., by $n + {}^3He \rightarrow p + {}^3H + 0.2$ MeV. The atoms were collisionally relaxed prior to reaction, yielding a wide translational energy distribution. This complication is avoided in the photolytic method of hot H-atom generation, first used for kinetic studies by Ogg and Williams.[5,6] For these early studies, H atoms were generated by photolysis of HI with the 253.7 nm line of a mercury lamp. Photolytic hot atom experiments have experienced a renaissance in recent years because of the advent of UV laser sources. Pulsed-laser photolysis allows the generation of high densities of fast atoms on a time scale much shorter than that of subsequent collisions. This method, combined with time-resolved detection by pulsed lasers, permits reaction studies to be performed under single-collision conditions.

Quick and Moore[7] were the first to apply pulsed-laser photolysis to the study of the $H + H_2$ reaction. The H atoms were generated by photolysis of HBr at 193 nm; coherent anti-Stokes Raman spectroscopy (CARS) was used to probe the H_2 product of both ineleastic and reactive collisions. Rotational and vibrational excitation of the product was observed, but not quantified. Shortly after this initial measurement, two groups reported quantitative internal state distributions of the HD product from the $H + D_2$ reaction.[8-11] Both groups used the fourth harmonic of a pulsed Nd:YAG laser ($\lambda = 266$ nm) to photolyze HI, generating H atoms with center-of-mass collision energies of 0.55 and 1.3 eV, corresponding to the production of $I^*(^2P_{1/2})$ and $I(^2P_{3/2})$, respectively. These energies are above the classical reaction barrier of 0.42 eV.[12-14] Gerrity and Valentini[8,9] (GV) detected the HD product with CARS, while Marinero, Rettner, and Zare[10,11] (MRZ) used (2 + 1) resonance-enhanced multiphoton ionization (REMPI). The results of these first quantum-state-specific measurements were in reasonable agreement, but there were deviations outside of the combined error bars, primarily in the $HD(v = 1)$ rotational distribution.

The CARS method has been applied to both reactive and inelastic scattering studies of $H + D_2$ at other collision energies, as well as to $D + H_2$ and $H + H_2$.[15-20] In the latter two reaction systems, evidence has been reported for scattering resonances, which are attributed to excitation of vibrational modes of the reaction complex. In another laser-based experiment[21,22] on the $H + D_2$ reaction, the HD_2 transition state has been detected directly via multiphoton ionization. Unfortunately, the structural features of this transient species have not yet been determined.

Differential cross sections of the hydrogen-atom hydrogen-molecule exchange reaction have also been experimentally probed.[23-34] These studies have employed a combination of crossed molecular beam techniques with time-of-flight mass spectrometry (TOF/MS) of the product. To date, these experiments have provided angular distributions with vibrational quantum-state resolution, but only limited rotational information has been obtained. Recently, Continetti, Balko, and Lee[31,32] have derived the most complete flux-velocity contour maps for the $D + H_2$ system at energies of 0.51 and 0.98 eV. Welge and co-workers[33,34] have demonstrated a novel TOF approach to obtain angular information on the D-atom product of the $H + D_2$ reaction. They employed a crossed beam setup, in which the D atom is detected by laser excitation to high Rydberg states and subsequently ionized by an electric field. Initial results, obtained for laboratory angles of 0° and 45°, show marked variations in the D-atom kinetic energy spectrum as a function of angle.

The inherent simplicity of the H_3 system makes it particularly amenable to theoretical treatment.[35-40] This simplicity arises from two sources: (i) the small number of electrons, which has made possible the calculation of the most

 0021-9606/89/247514-16$02.10

accurate potential energy surface [12,41–44] (PES) for any neutral reactive system, and (ii) the lightness of the nuclei, which results in a large spacing between rovibrational levels, thereby limiting the number of accessible product quantum states (channels). Additionally, the small number of classical degrees of freedom (present in any triatomic system) facilitates quasiclassical trajectory (QCT) calculations. The $H + H_2$ reaction (and its isotopic analogs) is therefore the benchmark system for theoretical studies of chemical reaction dynamics. Both QCT[45–51] and quantum mechanical[52–68] (QM) studies have been published, predicting product-state distributions as well as other attributes of this reaction system. Recently, the first fully converged quantal calculations[67,68] were reported for $H + H_2$ at total energies of 0.9–1.4 eV. Much of the theoretical work still awaits comparison with experimental studies.

Whereas the theoretical calculations provide complete product-state distributions, the initial experimental data sets were incomplete because of sensitivity limitations imposed by the CARS and REMPI detection schemes. We succeeded in improving the detection sensitivity of REMPI (Sec. II) to $\sim 1\times 10^6$ molecules/cm^3 per quantum state, allowing the observation of HD product from $H + D_2$ reaction channels with partial cross sections as small as 5×10^{-4} Å^2, as estimated from QCT[48] calculations. The experimental setup is conceptually identical to that used in the earlier work of MRZ.[10,11] We recently reported the first complete HD($v = 1, 2$) rotational distributions.[69] The new measurements reported here, consisting of the HD($v = 0, J$) rotational distribution and the HD($v = 0$–2) vibrational distribution, complete the study of the $H + D_2$ reaction at center-of-mass collision energies of 0.55 and 1.3 eV. Several control experiments are described in Sec. III. The observed distributions are discussed and compared to previous results and theoretical predictions in Sec. IV.

II. EXPERIMENTAL

An overview of the experimental setup is shown in Fig. 1; the vacuum chamber is detailed in Fig. 2. D_2 and HI are premixed and introduced into a high vacuum chamber via a capillary nozzle. The reaction is initiated ~ 2 mm below the nozzle by laser photolysis of HI at 266 nm. After a delay of ~ 55 ns, the HD product is state-selectively ionized via $(2 + 1)$ REMPI. The HD^+ ions are mass-selectively detected in a shuttered time-of-flight mass spectrometer.[70]

A. Reagents

HI (Scott Gases; stated purity: 99.95%) is purified in a glass bulb by a freeze–pump–thaw cycle in order to remove the H_2 contaminant; most of the I_2 contaminant remains in the HI cylinder. The purified HI and D_2 (Cambridge Isotopes; stated purity: 99.7% D) are premixed in the ratio 1.0:3.5 and stored in a sample cylinder that is Teflon lined to minimize wall exchange reactions. Exposure of the mixture to light is avoided to suppress HI decomposition. In our study of the $H + HI$ reaction[71,72] using the same apparatus, it was determined that after ~ 10 h of storage the partial pressure of H_2 caused by HI decomposition was less than 2% of the HI pressure.

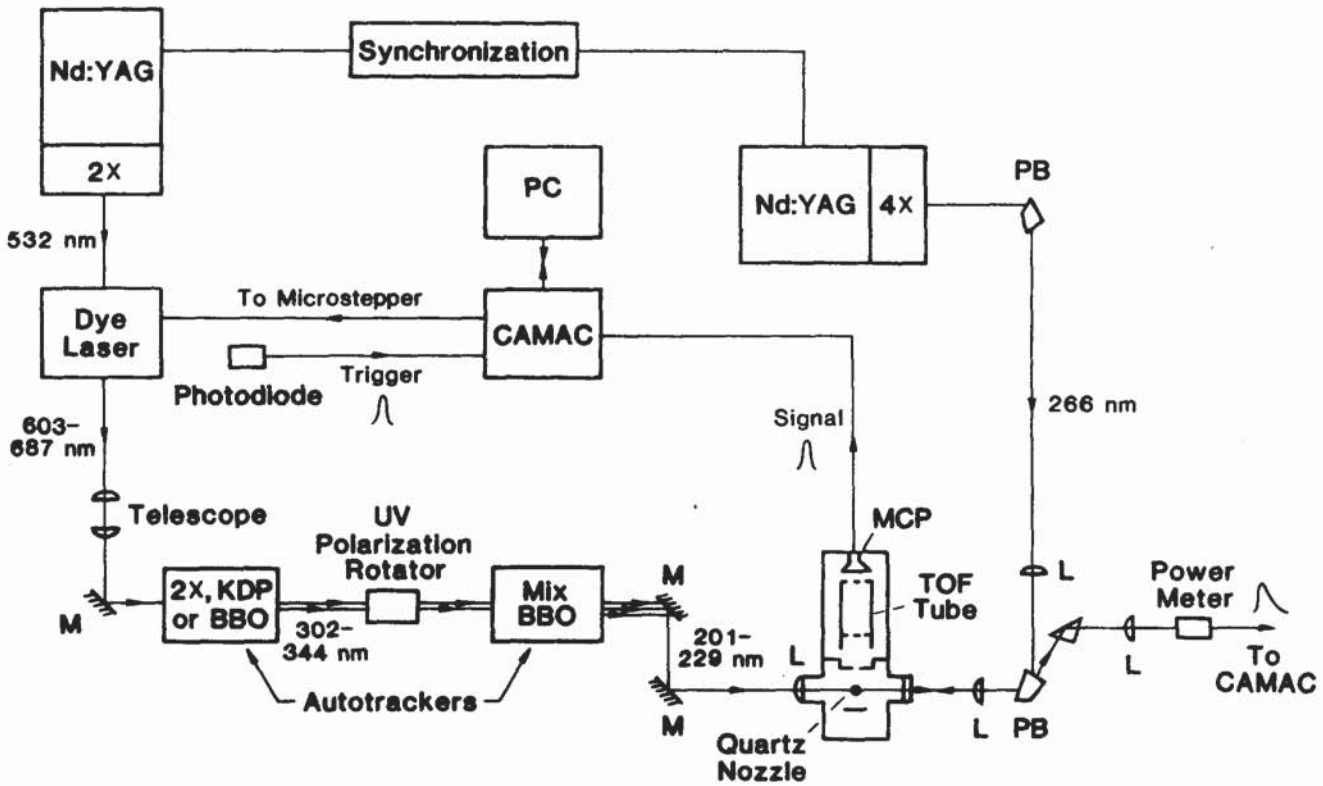

FIG. 1. Schematic diagram of the experimental configuration: M = dichroic mirror; L = lens; PB = Pellin–Broca prism; MCP = multichannel-plate detector; and PC = personal computer.

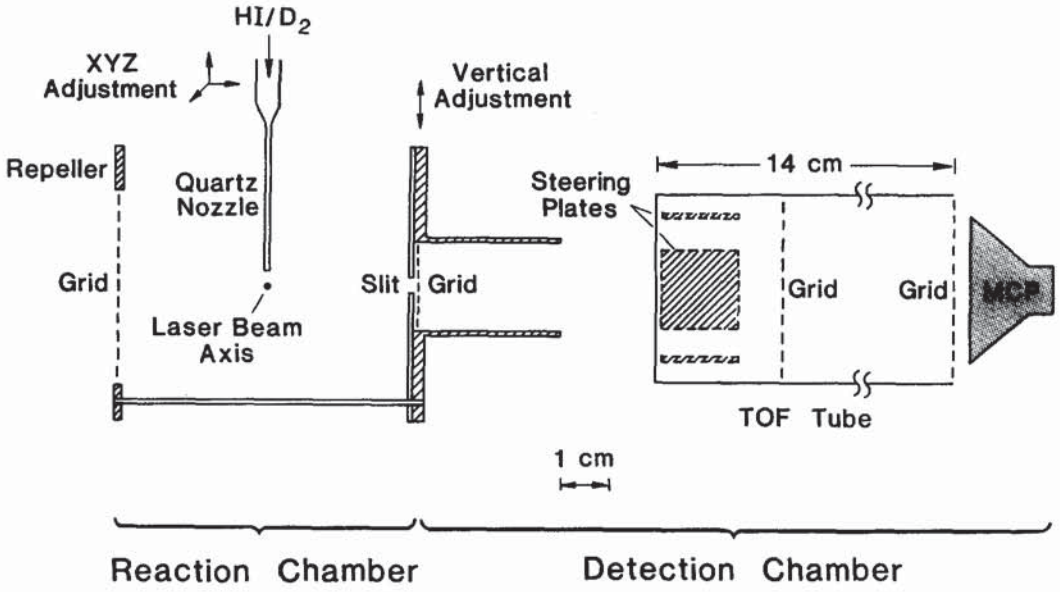

FIG. 2. Expanded view of the reaction and detection chambers.

The mix is introduced into the reaction chamber via a vertical quartz capillary nozzle ($\sim$0.8 mm diam. orifice), which is coated with graphite and electrically grounded in order to minimize electrostatic charging. A bellows metering valve allows fine regulation of the reagent pressure to 11–15 Torr in the line leading to the nozzle. The local density $\sim$2 mm below the nozzle corresponds to a pressure of less than 10 mTorr. Since the pressure drop occurs over the entire length of the capillary ($\sim$1 cm), the flow of the reagents should be effusive. This conjecture was tested by flowing 11 Torr of $\sim 10^{-2}\%$ D_2 in He through the nozzle and measuring the $D_2(v=0)$ rotational distribution by REMPI. The D_2 was determined to be at room temperature (298 K), verifying that the capillary nozzle operates in the effusive flow regime.

The reaction chamber is constructed from a six-way cross pumped by a liquid-nitrogen (LN_2)-trapped, 6 in. diffusion pump (DP) (NRC, Santovac oil) backed by an LN_2-trapped rotary pump (Welch, Model 1397). The base pressure is $\sim 5\times 10^{-8}$ Torr. The nozzle directs the reagent gases directly into the LN_2 trap. During reagent flow, the pressure in the reaction chamber rises to $\sim 2\times 10^{-4}$ Torr.

B. Lasers: HI photolysis and HD REMPI detection

Two laser beams that are counterpropagating perpendicular to the nozzle intersect the effusive reagent beam $\sim$2.0 mm below the nozzle tip (Fig. 2). The nozzle is mounted on an x–y–z translation stage to allow its positioning with respect to the laser beams.

The horizontally polarized fourth harmonic (266 nm) of a Nd:YAG laser (Spectra-Physics, DCR-1A or DCR-11; 10 Hz) photolyzes the HI. The resulting H atoms have center-of-mass collision energies of 1.3 and 0.55 eV, corresponding to the production of $I(^2P_{3/2})$ and spin–orbit excited $I^*(^2P_{1/2})$, respectively. The I*:I branching ratio[73] is 0.36:0.64. Typical photolysis laser conditions are $\sim$3.5 mJ/pulse of energy collimated into a beam of $\sim$2.5 mm diameter. At this power density ($\sim$14 MW/cm^2), measurements and calculations both indicate that less than 10% of the HI in the interaction volume is photolyzed. It is not possible experimentally to saturate the HI photolysis at 266 nm so as to obtain a higher concentration of H atoms. Higher pulse energies result in the appearance of color centers and bulk damage in all optical components in the beam path. An increase in the power density through reduction of the laser beam diameter creates problems with HD product flyout and substantial background ion formation.

The probe laser is fired $\sim$55 ns after the photolysis laser to detect the nascent HD product by (2 + 1) REMPI. Figure 3 depicts the potential energy curves relevant to the detection process. Absorption of two $\sim$210 nm photons induces HD to undergo a Q-branch transition from the (v, J) rovibrational level of the HD $X\,^1\Sigma_g^+$ state to the $(v'_E=0, J'=J)$ rovibrational level of the $E, F\,^1\Sigma_g^+$ double minimum state. The electronically excited HD molecules are subsequently ionized by absorption of an additional photon from the same laser pulse. Here, $v'_E=0$ denotes the lowest vibrational level of the inner well of the E,F state (see Fig. 3).

The probe-laser system consists of a pulsed (10 Hz) Nd:YAG-pumped dye laser (Spectra-Physics, DCR-3G, PDL-1; dye: Exciton, R640/DCM), and frequency-doubling and mixing stages (INRAD, Autotracker II). The dye laser light (603–687 nm) is frequency doubled in β-barium borate (BBO, 40° cut).[74] The residual dye laser light is frequency mixed with the doubled light in a second BBO crystal (70° cut) yielding 1.0–3.0 mJ per pulse of horizontally polarized radiation at 201–229 nm. Two dichroic mirrors (Virgo Optical) separate the VUV radiation from the other harmonics and steer the beam into the reaction chamber, allowing optimization of the probe laser position with respect to the photolysis laser and the capillary nozzle. The probe beam is focused (Esco, Suprasil B, $f=125$ mm) to a spot size of $\sim 100\,\mu$m, giving a power density of $\sim$4 GW/cm^2 in a 5 ns pulse.

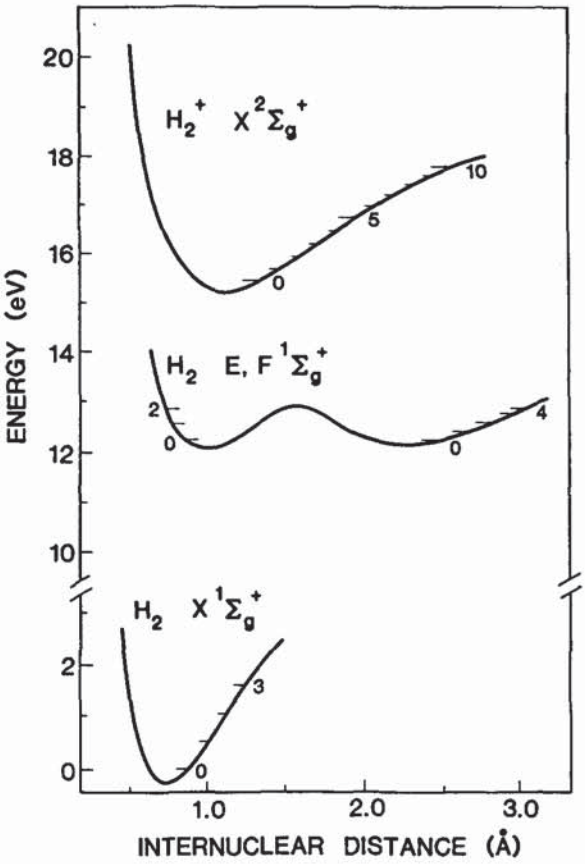

FIG. 3. Potential energy diagram of the relevant levels for (2 + 1) REMPI detection of molecular hydrogen.

C. Ion detection

The HD^+ ions are mass-selectively detected in a shuttered TOF/MS,[70] which is located in the detection chamber. The detection chamber is separated from the reaction chamber by a slit and pumped by an LN_2-trapped, 4 in. diffusion pump (Varian, Santovac oil). The base pressure in the detection chamber is $\sim 3\times 10^{-8}$ Torr. The reaction and detection chambers are differentially pumped in order to maintain an adequately low pressure in the latter chamber for the operation of the ion detector[75] and to ensure collision-free conditions in the TOF/MS. During reagent flow, the pressure ratio between the two chambers is ~ 100, with the detection chamber pressure increasing to $\sim 2\times 10^{-6}$ Torr.

The ions are formed between two charged plates (~ 190 V/cm), which accelerate the ions through the slit and into the detection chamber. The ions pass by two sets of orthogonal steering plates before entering the TOF tube (14 cm length; ~ -330 V). The drift region is defined by two grids held at the potential of the TOF tube. The effects of stray fields are minimized by floating all surfaces in proximity to the ion trajectory. The ions impinge on a CEMA detector (multichannel plate; Galileo Corp.), which has a gain of $\sim 2\times 10^7$ electrons/ion (operating voltage: -2000 V) allowing single ion detection. Typical arrival times with respect to the probe laser pulse are $\sim 1.4\,\mu$s for H_2^+, $\sim 1.7\,\mu$s for HD^+, and $\sim 2.0\,\mu$s for D_2^+.

The voltage on one of the steering plates is pulsed so that it acts as an ion shutter that is open to transmit only the ions of interest. This pulsed plate, which effectively makes the apparatus a tandem TOF/MS, improves the detection sensitivity by more than an order of magnitude.[70]

The ion signal from the CEMA detector is recorded by a computer-interfaced CAMAC system that gates (45 ns width) and integrates the HD^+ ion current. The spectra are recorded with a time constant of 2 to 10 s. The data are processed by an IBM PC XT computer.[76] Typical spectra are shown in Fig. 4.

III. RESULTS

As discussed in Sec. III A, several studies were performed to ensure that the observed signal was from the nascent HD product of the H + D_2 reaction. The distributions are presented in Sec. III B.

A. Control and optimization measurements

1. Mix ratio study

No change in the HD($v = 1$, J) product distribution was observed for several HI:D_2 concentration ratios between 1:1 and 1:7. The HI:D_2 ratio of 1:3.5 gave the highest product yield and all measurements were consequently performed with this ratio.

2. Time delay study

The time delay between the photolysis and probe laser pulses must be sufficiently long that an observable concentration of HD product is formed, but short enough to avoid product flyout and collisional relaxation of the reactants and products. With the maximum possible speed of ~ 9300 m/s, the HD molecules travel 1.3 mm (half the photolysis-laser spot size) in ~ 140 ns; this constitutes the upper limit of the delay time for which product flyout is negligible. Collisional relaxation of the hot H-atom reagent and the HD product must also be considered. For H atoms moving with a speed of 17 660 m/s (1.3 eV center-of-mass collision energy) in 10 mTorr of room temperature H_2 (27 Å^2 hard-sphere collision cross section),[77] the average time between collisions is ~ 460 ns. Under the same conditions, HD traveling at the maximum speed of 9300 m/s undergoes on average one hard-sphere collision each ~ 900 ns. The delay between the lasers must be shorter than all of these estimated maximum values.

Product rotational quantum-state distributions were recorded over a broad range of delay times between the photolysis and probe lasers. Under our experimental conditions, the HD^+ signal reaches a maximum magnitude at a delay of ~ 60 ns. The distribution does not change for delay times of less than 110 ns, a fact that is in good agreement with the flyout time calculated above (140 ns). A 55 ns delay was generally used, ensuring that product flyout, as well as product and H-atom collisional relaxation, is negligible.

3. Calibration of the (2+1) REMPI detection scheme

A major effort has been directed toward calibration of the HD (2 + 1) REMPI detection process in order to deter-

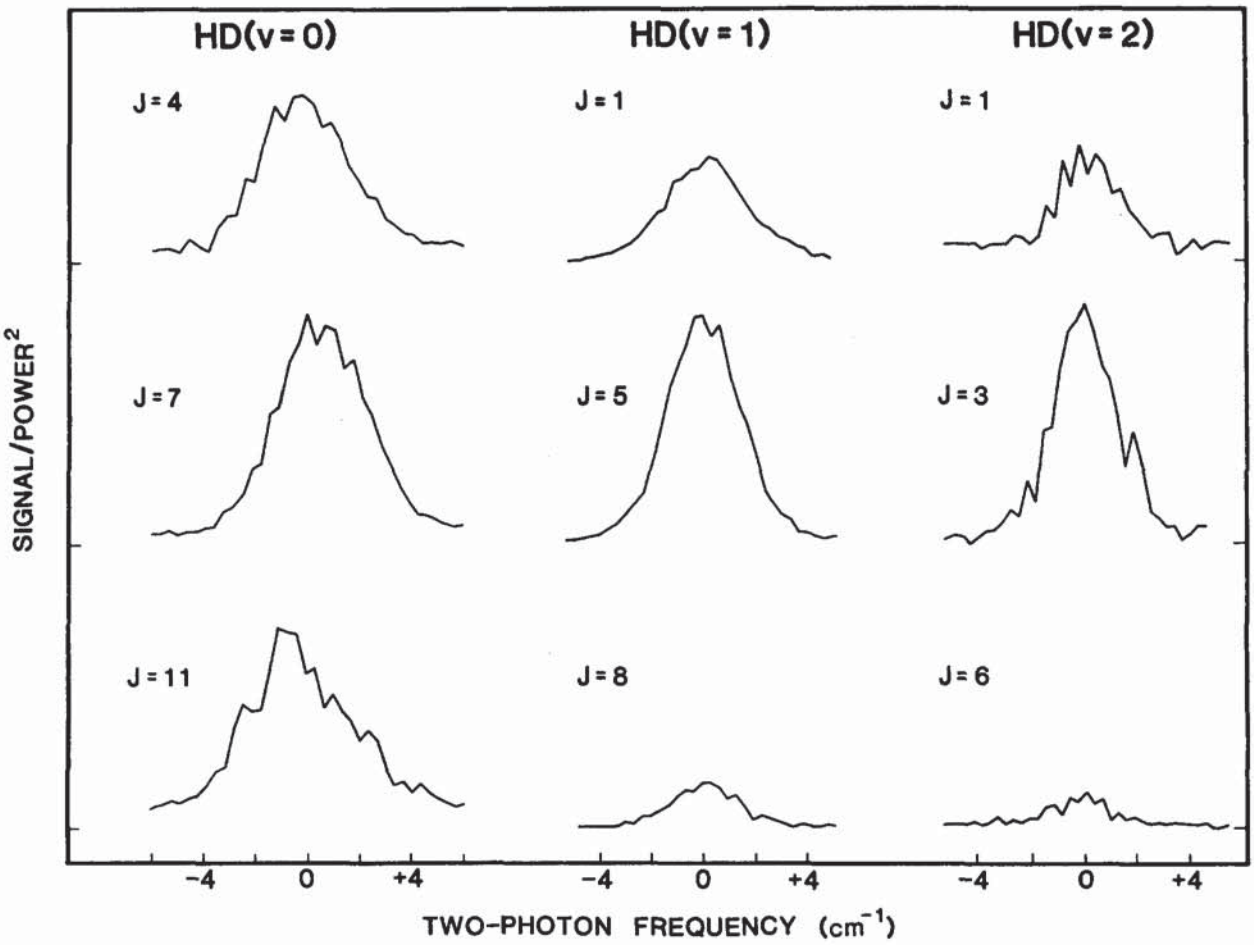

FIG. 4. Power-corrected REMPI signal for the HD product from the H + D_2 reaction.

mine quantitatively the relationship between ion signals and relative quantum-state populations. This study has been published elsewhere.[78,79] Briefly, an effusive, high temperature nozzle was constructed to excite HD molecules into high rovibrational levels with a thermal population distribution. A comparison of the integrated, power-corrected ion signals to the known Boltzmann population distribution yields any necessary correction factors.

The results of the calibration are:

(1) There is no J dependence in $v = 0$ and 1; hence, all rotational correction factors for these vibrational levels are unity.

(2) There is a slight J dependence in $v = 2$; rotational correction factors are listed in Table I.

(3) The Q-branch transition from the $X\ ^1\Sigma_g^+$ ($v = 2$, $J = 1$) state to the $E,F\ ^1\Sigma_g^+$ ($v'_E = 0, J' = 1$) state is blended in the (2 + 1) REMPI detection scheme. Therefore, the population of the ($v = 2, J = 1$) level cannot be reliably determined.[80]

(4) There is a significant v dependence to the ion signal; the vibrational correction factors are listed in Table II.

(5) The ionization step is saturated under the given experimental conditions.

(6) The two-photon transition is partially saturated. While this will affect a comparison between the experimental correction factors and theoretically calculated transition moments,[78] it is of no consequence for the present experiment.

4. Polarization study

The reaction process can introduce an anisotropic M_J distribution, i.e., alignment, of the product molecules. As shown by Kummel, Sitz, and Zare,[81] the transition probability of (2 + 1) REMPI is sensitive to the ground-state M_J distribution. For an aligned molecular sample, the REMPI

TABLE I. Rotational correction factors for the transition HD $E,F\ ^1\Sigma_g^+$ ($v'_E = 0, J' = J$) − $X\ ^1\Sigma_g^+$ ($v = 2, J$).

J	Multiplicative correction factor
0	[1.17][a]
1	[1.16][a]
2	1.14 + 0.11
3	1.12 ± 0.10
4	1.07 ± 0.05
5	0.98 ± 0.05
6	0.94 ± 0.06
7	0.85 ± 0.08
8	0.80 ± 0.12

[a] Extrapolated from a least squares regression analysis based on the $J = 2$–8 correction factors (Ref. 78).

TABLE II. Vibrational correction factors for the two-photon transition HD $E,F\,^1\Sigma_g^+(v'_E=0)-X\,^1\Sigma_g^+(v)$.

v	Relative detection sensitivity
0	1.00
1	2.4 ± 0.4
2	2.9 ± 0.8

ion signal is not directly proportional to the population. Since the above calibration determines the relationship between ion signals and quantum-state populations for an unaligned (thermal) HD sample, it is important to investigate whether any product alignment is produced in the $H+D_2$ reaction under the present experimental conditions.

As shown by van Veen *et al.*,[82] the photodissociation of HI involves transitions to four electronic surfaces. The fast H-atom fragments correlated with the production of ground-state I arise from an almost purely perpendicular transition at 266 nm; the slow H atoms, produced in coincidence with I*, result from a primarily parallel transition. Since the photodissociation is prompt, there is a strong correlation between the nature of the electronic transition and the spatial distribution of the photofragments. The spatial probability distributions of the fragments are cylindrically symmetric about the polarization axis of the photolysis laser, with $\sin^2\Theta$- and $\cos^2\Theta$-shaped lobes for the fast and slow channels, respectively, where Θ is measured from the polarization axis. The anisotropy of the H-atom angular distribution may be mapped into an anisotropic M_J distribution of the HD product.

As will be discussed later (Sec. IV), the 0.55 eV channel contributes significantly only to the HD($v=0$) product, while the 1.3 eV channel contributes to all product vibrational states. Because the two channels correspond to different H-atom spatial distributions, product alignment may vary with v. Thus, it is necessary to check for alignment effects in both HD($v=0$) and HD($v=1$ or 2). HD($v=0$ and 1) rotational distributions were recorded for vertical and horizontal photolysis-laser polarizations, while leaving the polarization of the probe laser fixed (horizontal). The rotation of the photolysis-laser polarization, i.e., of the axis of cylindrical symmetry, will cause a change of the ion signal in the presence of nonzero alignment.

The rotational distributions for the two polarization geometries were found to be the same to within experimental accuracy, i.e., there are no alignment effects. Therefore, the results of the high-temperature oven calibration can be directly applied to the reactive distributions. This is not surprising in light of the saturation of the two-photon transition, which diminishes any M_J dependence of the REMPI signal,[81] and the experimental geometry, which has no well-defined initial direction for the relative velocity of the reagents.

5. Prompt-reaction background

HD^+ ions are observed in the absence of the photolysis laser.[80] This is caused by probe-laser induced photolysis of HI, i.e., the probe laser both generates fast H atoms and detects the HD product formed during a single laser pulse. This probe-laser induced, or "prompt," signal must be subtracted from the total signal in order to obtain the 266 nm-induced signal. It is not adequate to correct for the prompt signal by operating the photolysis laser at 5 Hz and the probe laser at 10 Hz and subtracting alternate shots because the photolysis beam partially depletes the HI present within the probe-laser volume. Such a correction scheme would overcompensate for the prompt reaction contribution to the HD signal.

Two methods have been used to obtain the 266 nm-induced distribution. The first method involves subtracting a fraction of the prompt reaction from the observed signal on a shot-by-shot basis. The fractional HI depletion by the 266 nm beam (F) is determined by measuring the 266 nm-induced reduction in the signal at a rotational level that is energetically accessible only by the prompt reaction. The spectral peaks are subsequently corrected for the prompt product in the following manner: with the photolysis laser operating at 5 Hz and the probe laser at 10 Hz, the signal without photolysis multiplied by ($1-F$) is subtracted from the signal with photolysis. The depletion factor F is measured prior to recording each distribution to ensure that no drift has occurred.

The second method used to correct for the prompt reaction involves switching the delay between the firing of the photolysis and probe lasers from $\sim$55 to $\sim$15 ns on alternate probe laser pulses. At the shorter delay, the signal contains contributions from both the prompt and 266 nm-induced reactions; the longer delay has the same prompt-reaction contribution, but has a larger 266 nm-induced signal because of product buildup. The ion signal at the short delay time is subtracted from that at the long delay (again, on a shot-by-shot basis); this difference contains signal exclusively from the 266 nm-induced reaction. With this method, *no assumptions are made concerning 266-nm depletion of the HI and long term drifts are minimized*. The results of measurements with the two methods agree very well. The second method, by virtue of its inherently greater reliability, was used in the majority of the measurements.

In order to illustrate the correction process, the HD($v=0, J=7$) spectral peak is shown in Fig. 5. Figure 5(a) shows the spectrum recorded at long delay time with contributions from both the probe-laser and the 266-nm photolyses. The spectrum in Fig. 5(b) recorded at short delay time is subtracted to give the residual [Fig. 5(c)], which corresponds to the 266 nm-induced reaction product only. As shown in the figure, the signal-to-noise ratio decreases in this process.

HD product from the prompt reaction is observed in $v=0$–3. Rotational distributions are reported in Ref. 80.

B. HD product distributions

The REMPI signal is a measure of the *density* of a given HD rovibrational state at the temporal and spatial position of the probe-laser focus. In the measurements of the reaction, the probe-laser focus is contained within the much larger photolysis beam. The time-delay study (Sec. III A 2)

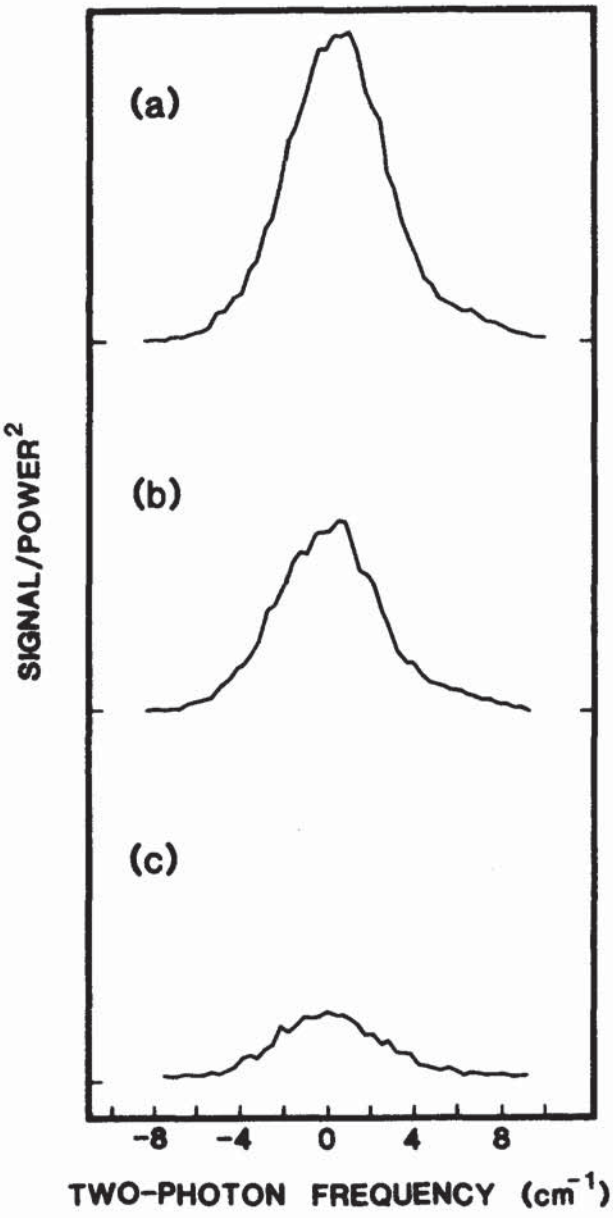

FIG. 5. Prompt-reaction correction procedure. The HD($v=0$, $J=7$) spectral peak is shown under different photolysis conditions: (a) measured at a long delay time ($\sim$55 ns) between the photolysis and probe laser pulses; (b) taken at a short delay time ($\sim$15 ns); and (c) result of the shot-by-shot subtraction of the spectrum at short delay from the spectrum at long delay. This latter spectrum contains product only from the 266 nm-induced reaction.

demonstrated that, under our experimental conditions, product flyout from the detection volume is negligible. Thus, for delay times of less than 110 ns, the detection sensitivity is independent of the velocity of the product molecules. The measured HD(v, J) density (ion signal) therefore corresponds to the time-integrated flux of reaction product into that quantum state. *The observed product rovibrational distributions are a direct measure of the relative rates of reaction into these states.*

1. Rotational distributions

The total energy of the system ($\sim$1.51 eV) enables the formation of HD product in the rovibrational states ($v=0$, $J=0$–15), ($v=1$, $J=0$–12), ($v=2$, $J=0$–8), and ($v=3$, $J=0$). HD($v=3$, $J=0$) is accessible only when the thermal spread in the center-of-mass collision energy ($\sim$0.08 eV) is taken into account. All rotational levels are observed, except $v=3$, $J=0$. For each vibrational band, we average more than 15 independent rotational distributions in order to obtain the final distribution. The population distributions are given in Tables III–V and displayed in Figs. 7–12. For comparison, previously published results[8, 9, 48, 53–55, 83] are included. The effect of the correction factors on the $v=2$ distribution is minor, as demonstrated in Fig. 6.

There is HD contamination ($\sim$0.4%) in the room temperature D_2 reagent. This contributes strongly to the populations in HD($v=0$, $J\leqslant 4$). The shot-by-shot correction to remove the prompt-product contribution to the measured distribution (Sec. III A 5, second method) simultaneously subtracts this HD contaminant contribution. The error bars for $v=0$, $J=0$–5 are relatively large because of the substantial HD impurity populating these levels. Of course, there is negligible room temperature background contribution to HD($v=1$) or HD($v=2$).

The populations of the levels HD($v=0$, $J=15$), HD($v=1$, $J=12$), and HD($v=2$, $J=8$) constitute the limit of the experimental detection sensitivity. The smallest detectable cross section is estimated to be $\sim 5\times 10^{-4}$ Å^2, based on the QCT partial cross sections.[48]

2. Vibrational and internal-energy distributions

The high-temperature oven calibration has made possible the determination of vibrational branching ratios, which are presented in Table VI. This table also lists predictions based on QCT calculations.[48] Both vibrational distributions are normalized to unity. The complete product distribution is plotted in a log-linear plot in Fig. 13, along with QCT and CARS[8,9,83] rovibrational distributions. The distributions are normalized to the sum of the populations of the common levels. The complete product distribution is also plotted as a function of internal energy[84] of the HD product in Fig. 14. The latter is normalized such that the sum over the populations of all rovibrational levels equals unity.

IV. DISCUSSION

We have measured the rovibrational distribution of the nascent HD product from the reaction H + D_2 → HD + D. Photolysis of HI at 266 nm generates fast H atoms with center-of-mass collision energies of 1.3 and 0.55 eV, correlated with the formation of I($^2P_{3/2}$) and I*($^2P_{1/2}$), respectively. Quantum-state-specific detection of HD is accomplished via (2 + 1) REMPI and TOF/MS. The detection scheme has been calibrated using a high-temperature, effusive nozzle. All energetically accessible HD levels [($v=0$, $J=0$–15), ($v=1$, $J=0$–12), and ($v=2$, $J=0$–8)] from the reaction have been observed.

The measured population distributions have contributions from two collision energies. The individual contribution of each collision energy cannot be isolated with the present experimental configuration. However, QCT partial cross sections[48] allow an estimate to be made of the relative impor-

TABLE III. HD rotational state populations[a,b] for $H + D_2 \rightarrow HD(v=0) + D$.

J	This work	GV(Refs. 8, 9, and 83)	BT(Ref. 48)	CS(Ref. 55)	SKL(Ref. 53)	BCPT(Ref. 54)
0	0.014(62)		0.018(03)	0.026	0.016	0.012
1	0.048(76)	0.041(05)	0.048(05)	0.069	0.063	0.036
2	0.075(75)	0.092(10)	0.067(06)	0.091	0.097	0.060
3	0.110(23)	0.124(13)	0.088(08)	0.094	0.127	0.082
4	0.111(20)	0.106(08)	0.082(08)	0.090	0.147	0.104
5	0.115(09)	0.116(06)	0.092(07)	0.096	0.153	0.125
6	0.107(08)	0.113(06)	0.098(06)	0.110	0.139	0.141
7	0.113(09)	0.098(06)	0.100(05)	0.122	0.109	0.145
8	0.105(12)	0.092(06)	0.117(05)	0.116	0.071	0.128
9	0.083(09)	0.086(06)	0.094(09)	0.083	0.036	0.092
10	0.058(06)	0.062(04)	0.083(05)	0.041	0.013	0.048
11	0.034(05)		0.061(05)		0.003	0.015
12	0.017(06)	0.013(03)	0.034(04)			0.002
13	0.006(03)		0.009(02)			
14	0.003(01)		0.0002(1)			
15	0.001(01)					

[a] Numbers in parentheses represent one standard deviation in the last digits, for example, 0.014(62) means 0.014 ± 0.062.
[b] The distributions are normalized to the sum of the (v, J) levels common with the reported distribution.

TABLE IV. HD rotational state populations[a,b] for $H + D_2 \rightarrow HD(v=1) + D$.

J	This work	GV(Refs. 8, 9, and 83)	BT(Ref. 48)	CS(Ref. 55)	SKL(Ref. 53)	BCPT(Ref. 54)
0	0.019(04)		0.022(08)	0.019	0.051	0.029
1	0.067(15)	0.088(12)	0.077(14)	0.057	0.189	0.084
2	0.100(17)	0.112(11)	0.078(13)	0.091	0.233	0.125
3	0.131(21)	0.147(23)	0.083(14)	0.114	0.202	0.150
4	0.156(18)	0.118(22)	0.148(18)	0.122	0.143	0.157
5	0.147(14)	0.141(11)	0.137(18)	0.119	0.088	0.157
6	0.130(13)	0.141(11)	0.143(18)	0.123	0.050	0.150
7	0.118(15)	0.088(11)	0.118(16)	0.135	0.024	0.120
8	0.073(15)	0.071(11)	0.106(15)	0.125	0.008	0.061
9	0.034(12)	0.049(11)	0.054(11)	0.070	0.001	0.012
10	0.014(08)		0.029(08)	0.014	0.0001	
11	0.006(08)		0.004(03)			
12	0.005(07)		0.0004(4)			

[a] Numbers in parentheses represent one standard deviation in the last digits, for example, 0.019(04) means 0.019 ± 0.004.
[b] The distributions are normalized to the sum of the (v, J) levels common with the reported distribution.

TABLE V. HD rotational state populations[a,b] for $H + D_2 \rightarrow HD(v=2) + D$.

J	This work	GV(Refs. 8, 9, and 83)	BT(Ref. 48)	CS(Ref. 55)	SKL(Ref. 53)	BCPT(Ref. 54)
0	0.082(14)		0.052(19)	0.021	0.063	0.061
1	0.133(31)		0.129(32)	0.064	0.240	0.173
2	0.198(18)	0.171(33)	0.143(39)	0.114	0.302	0.255
3	0.208(22)	0.186(39)	0.143(39)	0.167	0.239	0.252
4	0.193(21)	0.159(35)	0.168(39)	0.207	0.109	0.153
5	0.114(13)	0.198(35)	0.207(46)	0.202	0.025	0.035
6	0.051(11)		0.078(26)	0.145	0.002	
7	0.016(12)		0.071(26)	0.081		
8	0.004(07)		0.010(07)	0.00003		
9			0.003(01)			
10			0.001(01)			

[a] Numbers in parentheses represent one standard deviation in the last digits, for example, 0.082(14) means 0.082 ± 0.014.
[b] The distributions are normalized to the sum of the (v, J) levels common with the present experiment.

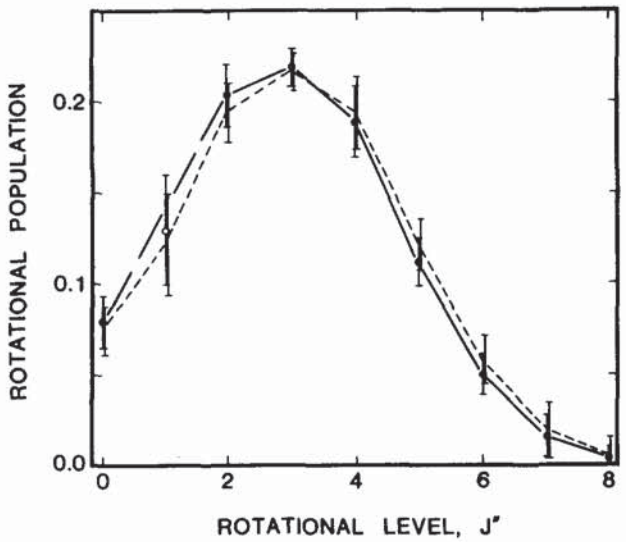

FIG. 6. Comparison of calibrated and uncalibrated rotational distributions of HD($v = 2, J$) from the H + D_2 reaction. The dashed line connects data points of the uncalibrated distribution, i.e., of the integrated ion signal without correction factors. The solid line connects points of the distribution corrected using the factors in Table I.

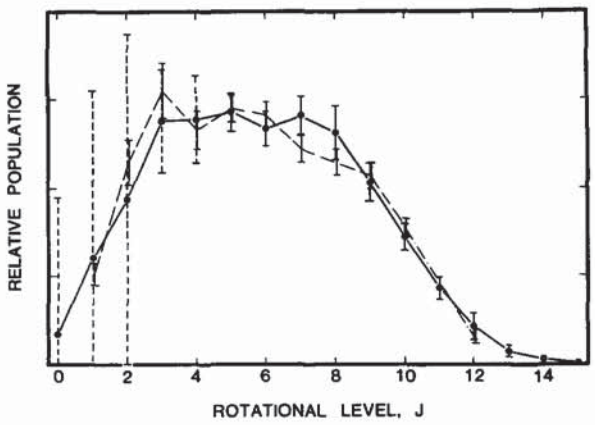

FIG. 7. Rotational distributions of HD($v = 0$) from the H + D_2 reaction. The data of the present study (solid line) and of CARS (Refs. 8, 9, and 83) (dashed line) are shown. Error bars represent one standard deviation. Because of HD contamination in the D_2 reagent, the error bars for HD($v = 0$, $J = 0$–4) are substantially enlarged and are dashed.

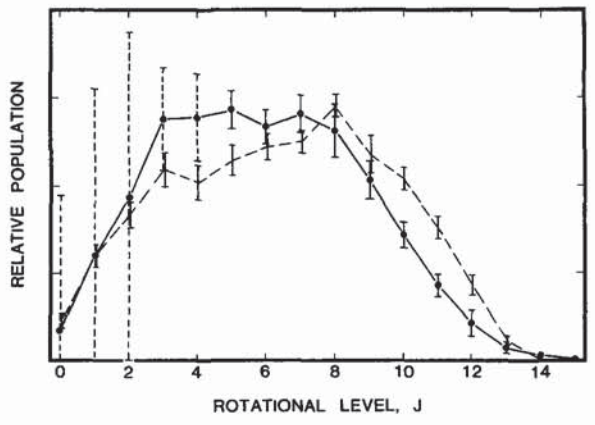

FIG. 8. Rotational distributions of HD($v = 0$) from the H + D_2 reaction. The data of the present study (solid line) and of BT (Ref. 48) (dashed line) are shown. Error bars represent one standard deviation. Because of HD contamination in the D_2 reagent, the error bars for HD($v = 0, J = 0$–4) are substantially enlarged and are dashed.

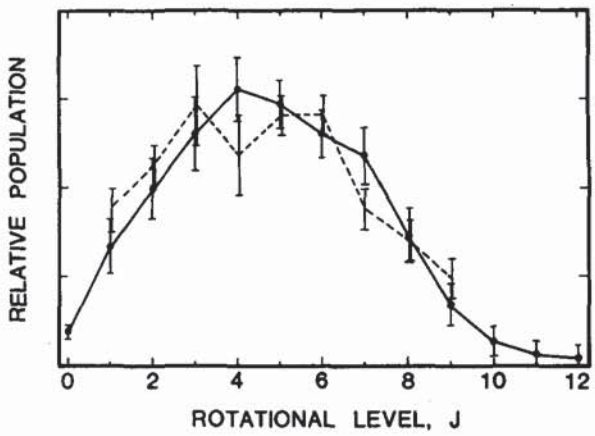

FIG. 9. Rotational distributions of HD($v = 1$) from the H + D_2 reaction. The data of the present study (solid line) and of CARS (Refs. 8, 9, and 83) (dashed line) are shown. Error bars represent one standard deviation.

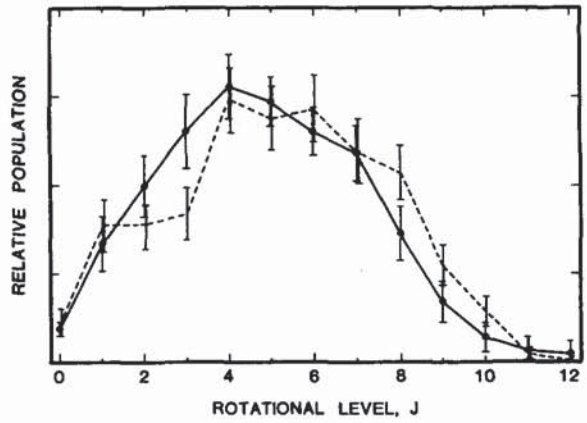

FIG. 10. Rotational distributions of HD($v = 1$) from the H + D_2 reaction. The data of the present study (solid line) and of BT (Ref. 48) (dashed line) are shown. Error bars represent one standard deviation.

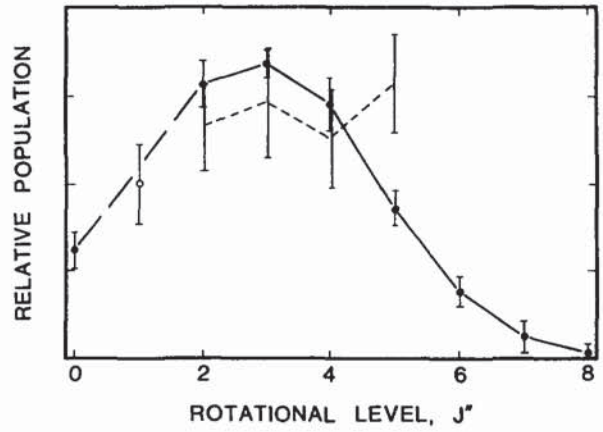

FIG. 11. Rotational distributions of HD($v = 2$) from the H + D_2 reaction. The data of the present study (solid line) and of CARS (Refs. 8, 9, and 83) (dashed line) are shown. HD($v = 2, J = 1$) is marked by an open circle because the population cannot be reliably determined by REMPI as discussed in Sec. III A 4. Error bars represent one standard deviation.

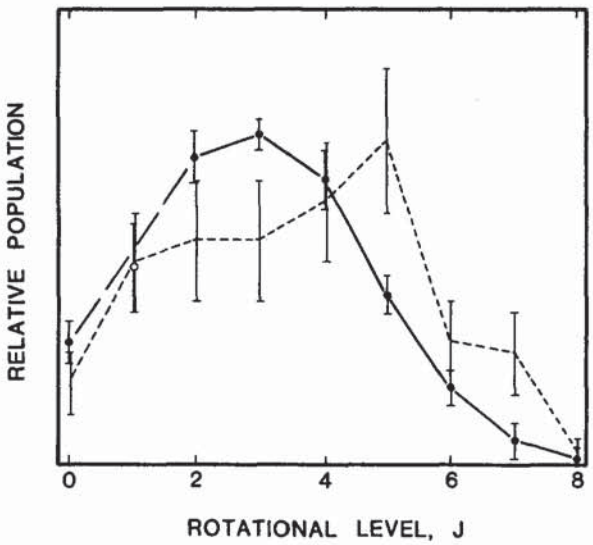

FIG. 12. Rotational distributions of HD($v = 2$) from the H + D_2 reaction. The data of the present study (solid line) and of BT (Ref. 48) (dashed line) are shown. HD($v = 2, J = 1$) is marked by an open circle because the population cannot be reliably determined by REMPI as discussed in Sec. III A 4. Error bars represent one standard deviation.

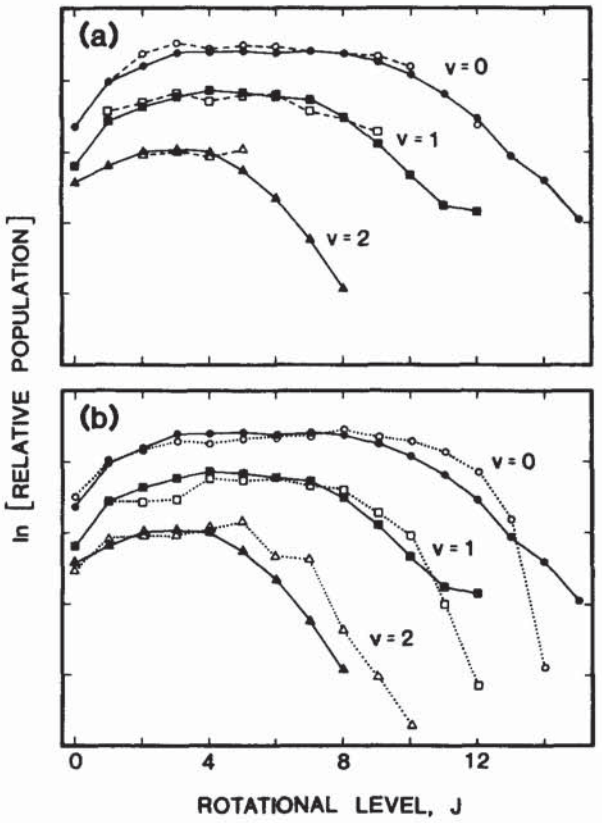

FIG. 13. Rovibrational distributions of the HD product from the H + D_2 reaction. The results of the present study (solid lines) are compared to previous data sets: (a) CARS (Ref. 83) (dashed lines) and (b) QCT (Ref. 48) (dotted lines). The rotational levels of $v = 0$ are denoted by circles, of $v = 1$ by squares, and of $v = 2$ by triangles.

tance of each channel to the observed distributions. The excellent agreement found between experimental and theoretical determinations of quantum-state distributions (Sec. IV B 3), as well as total reaction cross sections,[85,86] substantiates this procedure. The highest energetically accessible HD levels for the reaction with the slow H atoms are ($v = 0$, $J = 6$) and ($v = 1$, $J = 3$). Since the fast H-atom channel can populate up to ($v = 0, J = 15$), ($v = 1, J = 12$), ($v = 2$, $J = 8$), and ($v = 3, J = 0$), the slow channel contributes to less than one-third of all accessible rovibronic product levels. For $v = 0$, the slow H-atom reaction cross section[48] is predicted to be 16% of the total cross section, while for $v = 1$ it diminishes to less than 6% of the total. In addition, the photolysis branching ratio dictates that the slow channel contains about one-third of the total atomic-hydrogen density. These facts, in conjunction with the low collision frequency that accompanies lower relative velocities, indicate that our measured distributions are dominated by the product formed via the 1.3 eV collision-energy channel.

A. Quantum-state distributions

From the HD product rovibrational distributions shown in Figs. 7 through 14, three observations can be readily obtained:

TABLE VI. Vibrational branching ratios for H + $D_2 \rightarrow$ HD + D.

Ratio	This work	QCT (Ref. 48)
[$v = 0/v = 1$]	4.1 ± 0.8	4.8 ± 0.2
[$v = 1/v = 2$]	6.9 ± 1.5[a]	4.8 ± 0.7
[$v = 0/v = 2$]	29 ± 8[a]	23 ± 3

[a] For the calculation of the $v = 2$ population, the population of the level $v = 2, J = 1$ is interpolated by linear surprisal analysis based on $J = 0$, 2–6 (see Sec. IV B 1 and Table III).

(a) Most of the available energy is channeled into product translation. More than half of the HD molecules are formed in states that correspond to product translational energies in excess of 75% of the total energy. The reaction is almost thermoneutral ($\Delta H^\circ = 0.04$ eV), so that ~98 % of the available energy originates as relative reagent translation. Thus, there is an approximate conservation of translational energy. The most probable value of the product translational energy distribution is at ~1. 1 eV, corresponding to ~85% of the center-of-mass collision energy.

(b) Overall, the reaction product is found to exhibit a relatively low degree of rotational excitation (Figs. 7–12). Rotational excitation decreases with increasing vibrational energy, a fact that can be seen in both the peak positions of the rotational distributions and in the first moments (Table VII).

(c) The vibrational branching ratio is a monotonically decreasing function of v (Table VI). For small amounts of internal excitation, comparison of nearly degenerate rotational levels in adjacent vibrational states reveals a pronounced bias against vibrational excitation. For example, the levels HD($v = 0, J = 9$) and HD($v = 1, J = 2$) are almost energetically degenerate; the population ratio, however, favors formation of the $v = 0$ product by roughly a factor of 4. This trend markedly diminishes as the internal energy increases.

The channeling of reagent translational energy predom-

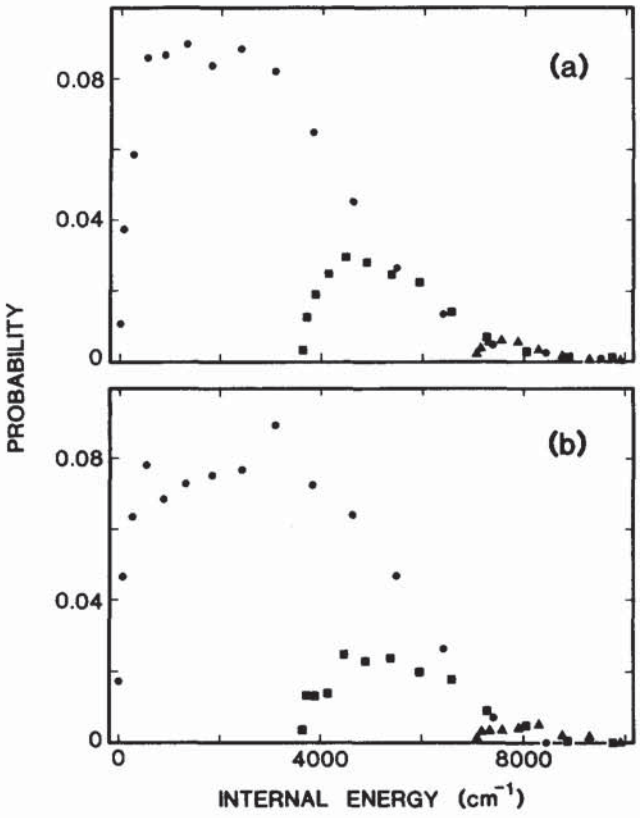

FIG. 14. Plot of relative population versus internal energy for the HD product from the H + D$_2$ reaction. The data shown are from (a) the present study and (b) QCT (Ref. 48). The rotational levels of $v = 0$ are denoted by circles, of $v = 1$ by squares, and of $v = 2$ by triangles.

inantly into product translation [point (a)] is a consequence of two intrinsic features of the H + D$_2$ reaction system: (1) the position of the reaction barrier, i.e., the H$_3$ PES is symmetric about the saddle point; and (2) the particular combination of masses, which gives a skew angle β in the mass-weighted coordinate system of 65.9° for H + D$_2$ (60° for H + H$_2$).

The low product rotational energy [point (b)] can be anticipated from the strong preference of the H$_3$ PES[12, 41–44] for collinearity at the saddle point.[87] The shift toward lower rotational excitation with increasing vibrational energy is consistent with a simple impulsive description of the reaction in which the excitation of higher vibrational levels results, on average, from collisions with smaller impact parameters.[88]

TABLE VII. First moments $\langle J \rangle$ of the rotational distributions for the HD product from H + D$_2$.

v	This work	QCT(Ref. 48)
0	5.9 ± 0.8	6.4 ± 0.2
1	4.8 ± 0.3	5.1 ± 0.3
2	2.9 ± 0.2[a]	3.6 ± 0.4

[a] The population of the level $v = 2$, $J = 1$ is interpolated by linear surprisal analysis based on $J = 0$, 2–6 (see Sec. IV B 1 and Table III).

The low propensity for vibrational excitation [point (c)] is also readily explained by the two features of the reaction system mentioned above in connection with point (a). In their QCT calculations, Blais and Truhlar[47] noted a tendency for adiabatic conservation of vibrational motion from reagents to products in the H + H$_2$ exchange reaction. This observation is consistent with the trend observed in the present experimental study. However, before our results can be uniquely attributed to vibrational adiabaticity, further experimental studies are needed, e.g., the effect of vibrational excitation of the D$_2$ reagent on the internal state distribution of the HD product must be systematically examined.

Table VIII summarizes the partitioning of the available energy (E) into the products of the H + D$_2$ reaction. In this table, f_i is the fraction of E partitioned into the ith degree of freedom, with $i = T$, V, or R, for translation, vibration, or rotation, respectively. In particular, we define

$$f_R = \sum_{v,J} P(v, J) E_R / E, \tag{1}$$

$$f_V = \sum_{v} P(v) E_V / E, \tag{2}$$

$$f_T = 1 - f_R - f_V, \tag{3}$$

where E_V (E_R) is the vibrational (rotational) energy and $P(v, J)$ is the population of the (v, J) rovibrational quantum state. The normalization assumed in Eqs. (1)–(3) is given by

$$\sum_{v} \sum_{J} P(v, J) = \sum_{v} P(v) = 1. \tag{4}$$

Observations (a), (b), and (c) discussed above are quantified in Table VIII.

A particularly interesting observation is that a constant fraction (~ 0.2) of $(E - E_V)$ appears in rotation (see the $\langle g_R(v) \rangle$ entries in Table VIII). This fraction $\langle g_R(v) \rangle$ is defined as

$$\langle g_R(v) \rangle = \left[\sum_{J} P(v, J) E_R / (E - E_V) \right] \sum_{J} P(v, J). \tag{5}$$

Therefore, conservation of energy dictates that $\sim 80\%$ of $(E - E_V)$ is channeled into translation. While intriguing, this result cannot be assumed to be general; it is most probably particular to our collision energy and mass combination.

TABLE VIII. Energy partitioning[a,b] in the HD product from H + D$_2$.

f_T	0.73
f_V	0.09
f_R	0.18
$\langle g_R(v = 0) \rangle$	0.20
$\langle g_R(v = 1) \rangle$	0.21
$\langle g_R(v = 2) \rangle$	0.17

[a] Definitions of f_i and $\langle g_R(v) \rangle$ are given in Eqs. (1)–(5) in the text.

[b] The population of the level $v = 2$, $J = 1$ is interpolated by linear surprisal analysis based on $J = 0$, 2–6 (see Sec. IV B 1 and Table III).

B. Comparison with other results

1. Surprisal analysis

In previous experimental investigations[8-11,83] of the H + D$_2$ reaction, the product rotational distributions were observed to be well described by linear surprisals. Theoretical studies[89-96] have also documented a tendency for linearity in the surprisal plots for reactions at low center-of-mass collision energies (<0.80 eV); however, at 1.3 eV collision energy significant deviations from linearity have been found. As this is the first experiment presenting complete rotational distributions at 1.3 eV collision energy, the theoretical prediction of surprisal plot curvature can be tested.

For the surprisal analysis two priors are used: (a) as in previous studies, a prior distribution is generated based on the constraint of conservation of total energy[97] and (b) the rotational distributions derived from a phase-space theory (PST) calculation[98-100] that includes conservation of total energy and angular momentum are used to define the priors. Note that only the 1.3 eV collision energy channel is considered in these analyses because the 0.55 eV channel represents only a minor contribution to the reaction product (see beginning of Sec. IV). Our surprisal results support the theoretical conjecture of deviations from linearity for high collision energies.

For an atom–diatom collision system at total energy E, the energy-conserving prior function,[93,97] $P^0(v, J; E)$, is given by

$$P^0(v,\ J;E) \sim (2J+1)(E - E_V - E_R)^{1/2}. \tag{6}$$

The surprisal[97] $I(v, J)$ is defined for a given product quantum state as

$$I(v,\ J) = -\ln[P(v,\ J)/P^0(v,\ J;E)]. \tag{7}$$

With these energy-conserving priors, plots of the surprisals versus g_R, the fraction of energy appearing in rotation [$g_R = E_R/(E - E_V)$], clearly exhibit curvature for all three observed vibrational bands (Fig. 15). For the low rotational levels ($J = 0$–6), it is possible to approximate the surprisal plots by straight lines, which yield the rotational surprisal parameters (slopes) Θ_R given in Table IX. As higher J levels are included, the slope and, therefore, Θ_R increase rapidly. Extrapolation of rotational level populations via linear surprisal analysis is unsuitable outside the range of $J \approx 0$–6. This behavior is in agreement with theoretical predictions,[95,96] especially with the QCT data of BT (Fig. 15). In contrast, our results contradict the previously published analysis of GV,[8,9,83] which suggested linear surprisals. However, note that Fig. 13 of GV omits the ($v = 0, J = 12$) point, which would substantially deviate from the reported linear surprisal plot.

PST may provide a more realistic method for construction of surprisal-analysis priors because of its simultaneous conservation of total energy and total angular momentum. Plots of $I(v, J)$ vs g_R based on PST prior distributions again exhibit curvature but of reduced magnitude when compared with statistical prior results. The surprisal parameters derived for $J = 0$–6 (Table IX) are similar for both the energy-conserving and the PST priors.

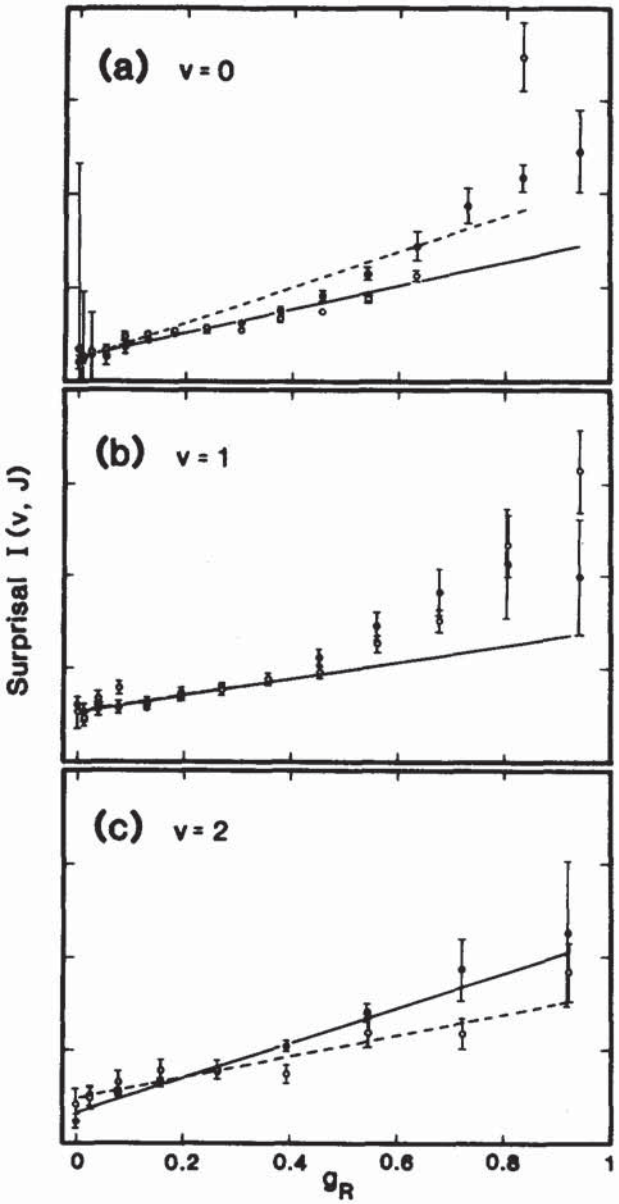

FIG. 15. Surprisal plots for the HD product of the H + D$_2$ reaction: (a) HD($v = 0$), (b) HD($v = 1$), and (c) HD($v = 2$). The experimental measurements are marked by solid circles (present study) and QCT results by open circles. The lines are derived from linear surprisal analyses based on $J = 0$–6 data for REMPI (solid line) and for QCT (dashed line). Error bars represent one standard deviation.

We conclude that linear surprisal analysis does not describe globally the H + D$_2$ reaction dynamics.

2. CARS

The present results are compared to the CARS distributions of GV[8,9,83] in Figs. 7, 9, and 11 for $v = 0$, 1, and 2, respectively. Since we measure relative populations, not absolute cross sections, the distributions are normalized so that the sum of the population of the common rotational levels is the same. The agreement is excellent.

For $v = 0$, the REMPI distribution (Fig. 7) extends from $J = 0$ to $J = 15$, the latter being the highest energetically accessible level. The CARS experiment reports $J = 1$–10 and $J = 12$. While the REMPI distribution is complete, its

TABLE IX. Rotational surprisal parameters for HD($J = 0$–6) from H + D_2.

	Energy-conserving prior			PST prior
v	This work	CARS(Ref. 8, 9, and 83)	QCT(Ref. 48)	This work
0	2.9 ± 0.6	3.1 ± 1.2	4.3 ± 0.6	3.3 ± 0.6
1	2.1 ± 0.4	3.1 ± 0.6	1.9 ± 0.9	1.5 ± 0.4
2	4.2 ± 0.4	1.4 ± 0.7	2.6 ± 0.5	3.8 ± 0.4

error bars for $J \leqslant 4$ are much larger than those for the CARS measurement. The shapes of the distributions are similar, aside from the dip at $J = 4$ in the CARS distribution. For $v = 1$, the lower detection sensitivity of CARS limits the range of reported levels to $J = 1$–9 (Fig. 9). In contrast, the REMPI distribution is complete, i.e., includes all energetically accessible $v = 1$ levels. The REMPI distribution is smooth and, as in $v = 0$, no evidence is found for the dip at $J = 4$ present in the CARS data. This observation is significant given the precedence for bimodal distributions in quantum theoretical treatments of D + H_2 and H + H_2 reactive scattering,[59,101] even at a single collision energy. Our measurements indicate that the HD($v = 1$) rotational distribution is definitely not bimodal. The branching ratio into HD($v = 2$) is small. Nevertheless, we again observe all levels permitted by energy conservation (Fig. 11). The CARS rotational distribution reports only the four most populated levels, $J = 2$–5, with error bars of 18%–22%. Meaningful comparison of our results with the CARS distribution is not possible.

The CARS rovibrational distribution is compared with our results in Fig. 13(a). It is not possible to extract relative vibrational cross sections from the CARS data since the rotational distributions are incomplete.

In conclusion, the previous discrepancy between the GV[8,9] and MRZ[10,11] HD($v = 1$) rotational distributions, which was largely caused by one deviant point [viz. the HD ($v = 1, J = 6$) population of MRZ], has been resolved. For 22 out of the 24 levels for which a comparison between REMPI and CARS is possible, the measured populations agree to within their experimental uncertainties.

3. Theoretical results

Although fully converged quantum calculations are not yet available at the translational energy used in the present study, the measured distributions may be quantitatively compared to the predictions of both distorted wave and QCT calculations. As in the previous comparison with the CARS results, the theoretical and experimental data sets are normalized to the sum of populations in the common levels.

Calculations based upon the application of the distorted-wave Born approximation to the H + D_2 reaction were performed by Salk, Klein, and Lutrus[53] (SKL), Bowers *et al.*[54] (BCPT), and Connor and Southall[55] (CS). The distributions obtained in this manner are listed in Tables III–V. The results of the calculations by SKL and BCPT are generally in poor agreement with the REMPI data, except for the HD($v = 1, J$) results of BCPT. The more recent calculations by CS, using a new static distortion potential, exhibit an improved agreement with REMPI. Note that the contribution of the 0.55 eV channel is corrected for these distributions according to the scheme proposed by CS.[55] The HD ($v = 0, 1; J$) distributions agree well but the HD($v = 2, J$) distribution is significantly too hot. From this comparison, we conclude that distorted wave calculations on the new state distortion potential, rival QCT calculations, in describing the H + D_2 reaction.

Blais and Truhlar[48] (BT) have performed three-dimensional QCT calculations under conditions simulating those of the present study. Their results are compared with our measured distributions in Figs. 8, 10, 12, and 13 and are listed in Tables III–V. For this comparison the theoretical cross sections must be converted into reaction rates, which constitute the experimentally determined quantity. This is accomplished by multiplying the theoretical cross sections for each H-atom channel by both the branching ratio for the relative H-atom density (0.64 for the fast channel and 0.36 for the slow channel) and the relative reagent velocity. The two distributions are subsequently summed in order to obtain quantities comparable with our experimental results. *The QCT rotational distributions are in remarkably good agreement with those derived from the REMPI measurements.* However, the QCT results appear to be slightly too hot rotationally, though for $v = 1$ the deviation is barely at the level of statistical significance. When the QCT distributions are shifted to lower J by roughly half a rotational quantum, the overlap of the distributions improves markedly. This trend towards slightly hot QCT distributions is confirmed by the first moments, which are tabulated in Table VII.

The above trend has also been observed in comparisons[52,101] between quantum-mechanical (QM) and QCT calculations. For the H + D_2 reaction at 0.55 eV collision energy Schatz compared QM calculations[39,52] using partial waves $J = 0$–16 with QCT calculations.[48] The distributions showed overall good, but not perfect, agreement, with a tendency for the QCT distributions to be slightly rotationally hot. A recent D + H_2 quantum mechanical calculation by Blais *et al.*[101] utilized $j = 0$–2 partial wave expansions for collision energies ranging from 0.70–1.05 eV. These results were compared to QCT distributions,[101] which were also limited to total angular momentum $j = 0$–2. The QM and QCT distributions were found to be in rather poor agreement, especially for HD($v = 1, J$); again, the QCT results were too hot rotationally. It is unclear to what extent the source of the discrepancy in this latter comparison is the

limited total angular momentum.

The vibrational branching ratios (Table VI and Fig. 13) exhibit good agreement between experiment and QCT. This observation is perhaps more unexpected than the agreement between the rotational distributions. The same QCT and QM calculations[52] for $H + D_2$ at 0.55 eV collision energy that compared favorably in their rotational distributions yielded rather poor agreement in the case of vibrational distributions. In particular, Schatz[52] found that the QCT and QM vibrational cross sections differed by $\sim 60\%$ for $v = 0$ and by several orders of magnitude for $v = 1$. Blais *et al.*[101] observed smaller differences ($\sim 11\%$ for $v = 0$ and $\sim 28\%$ for $v = 1$) in their calculations on the $D + H_2$ system at relative translational energies between 0.70 and 1.05 eV. While we observe better agreement with QCT predictions than either of the above QM calculations, the results of these three studies are not directly comparable as they pertain to different isotopic variants and collision energies.

The agreement between the present results and the predictions from QCT calculations is impressive. We also note that the QCT thermal rate constants[102] at 200–600 K for $D + H_2$ are in excellent accord with experiment.[103,104] However, such close agreement is not to be expected in all cases of the $H + H_2$ reaction family. For example, QCT thermal rate constants[105] calculated for the reaction of muonium [a light (0.113 amu) hydrogen-like atom in which the proton is replaced by a positive muon] with H_2 are one to two orders of magnitude larger than the experimental values.[106,107]

The accuracy of QCT calculations depends on the validity of neglecting quantum behavior in the reactive scattering process. In particular, QCT calculations neglect tunneling and changes in zero-point energy (ZPE) in going from reactants to products. These two processes are of opposing nature in that tunneling *decreases* the effective barrier to reaction with respect to the classical barrier, while the change in ZPE *increases* the effective barrier. The error introduced by neglect of these effects will be most pronounced for low translational energies with respect to the reaction barrier. The degree to which these errors will cancel will be determined by the particular mass combination. The above argument suggests that, as the collision energy is increased, the agreement between QCT and experiment should improve. This prediction is confirmed by a recent modeling[108] of our prompt-reaction $HD(v = 1)$ rotational distribution (1.5 and 2.25 eV collision energies).

It must be noted that QCT calculations also neglect the effect of reactive scattering resonances[109] in which a quasi-bound collision complex is vibrationally excited—a topic of active experimental[19,20] and theoretical[64,66–68] investigation for the hydrogen-atom hydrogen-molecule exchange reaction. We make no attempt to address this issue here.

An additional complication inherent in the QCT method is the binning procedure, that is, the assignment of reactive trajectories to specific quantum states.[47,97,110] In the QCT calculations of BT, the vibrational action j_v is divided by $\hbar$ to define the continuous vibrational quantum number v_c and the rotational action j_R, decreased by $1/2\,\hbar$, is divided by $\hbar$ to define the continuous rotational quantum number J_c. Subsequently, quadratic-smooth sampling (QSS) is used to assign probabilities that v_c and J_c are associated with neighboring quantum-state bins. Truhlar *et al.*[111] have presented arguments that QSS provides the most accurate correspondence between v_c and v and between J_c and J.

It is possible that the binning procedure is responsible for all or part of the discrepancy between QCT and experimental rotational distributions. We offer another possible explanation: the partial cancellation of opposing quantum-mechanical effects, tunneling and ZPE change, could cause the QCT rotational distributions to be slightly hotter than experimentally observed.[112] The $H + D_2$ reaction is described by the well-studied H_3 surface.[12–44] This PES has a strong preference for collinearity at the saddle point.[87] The barrier to reaction is ~ 0.42 eV for collinear approach and increases to ~ 1.3 eV for an approach perpendicular to the H–H bond axis. Most trajectories at 1.3 eV collision energy are well above the barrier and QCT calculations are expected to provide a reasonably accurate approximation to the forces experienced by the particles.[111] However, the reaction barrier plays a significant role for trajectories with strongly bent collision geometries and these classical trajectories are likely to be in error because of the neglect of tunneling and the change in ZPE. When tunneling constitutes the smaller of the two effects, the contribution to reaction from trajectories close to the barrier will be too large because trajectories with less than the zero-point energy in modes perpendicular to the reaction coordinate will be reactive. Because such bent configurations lead predominantly to formation of highly rotationally excited product molecules,[88] QCT calculations overestimate the populations of high J levels under these conditions. This is in accord with the trend observed in the present experiment. Assuming that the binning procedure is not responsible for the observed QCT–experiment discrepancy, this suggests that the neglect of ZPE change in the course of the $H + D_2$ reaction is more important than the neglect of tunneling at these collision energies.

Further experimental and theoretical studies are required at different collision energies and mass combinations in order to sort out the conditions for which QCT provides an accurate description of the $H + H_2$ reaction dynamics.

V. CONCLUSIONS

We have measured populations for all energetically accessible HD product levels for the $H + D_2$ reaction. This study represents the first determination of rovibrational distributions for the hydrogen-atom hydrogen-molecule exchange reaction that rival theory in their completeness. There is an approximate conservation of translational energy from reagents to products; most of the available energy is channeled directly into product translation (73%), while 18% appears in HD rotation and only 9% in HD vibration.

The CARS data of GV[8,9,83] for the HD internal state distribution are in excellent agreement with our results for those levels where direct comparison is possible. Our distributions are not described accurately by means of linear surprisal theory.

Both the QCT[48] rotational and vibrational distributions are in remarkably good agreement with those derived from the present REMPI measurements, although the QCT rota-

tional distributions are slightly too hot. This good agreement may reflect the fact that most trajectories cross the PES at translational energies well in excess of the reaction barrier, so that QM effects are negligible. The minor discrepancy between QCT rotational distributions and the present results may result all or in part from errors in the QCT binning procedure and/or from the incomplete cancellation of two opposing QM effects, tunneling and changes in ZPE along the reaction path. Further experimental and theoretical studies are required to determine the relative importance of QM effects.

ACKNOWLEDGMENTS

We thank R. S. Blake and M. A. Buntine for experimental assistance and are grateful to A. C. Kummel, G. C. Schatz, G. O. Sitz, and P. H. Vaccaro for many useful discussions. We also thank M. J. Bronikowski and R. Zhang for help with the PST calculations. Graduate fellowships are gratefully acknowledged by K.-D. R. (Deutscher Akademischer Austauschsdienst, Jahresstipendium 1984/5; Rotary Foundation, 1985/6) and D. A. V. K. (National Science Foundation). This project is supported by the National Science Foundation under Grant No. NSF CHE 87-05131.

[1]G. W. Flynn and R. E. Weston, Jr., Annu. Rev. Phys. Chem. **37**, 551 (1986).
[2]I. G. Campbell, in *Advances in Inorganic Chemistry and Radiochemistry*, edited by H. J. Emeleus and A. G. Sharppe (Academic, New York, 1963).
[3]R. Wolfgang, Prog. React. Kinet. **3**, 97 (1965).
[4]R. Wolfgang, Annu. Rev. Phys. Chem. **16**, 15 (1965).
[5]R. A. Ogg, Jr. and R. R. Williams, Jr., J. Chem. Phys. **13**, 586 (1945).
[6]R. A. Ogg, Jr. and R. R. Williams, Jr., J. Chem. Phys. **15**, 691 (1947).
[7]C. R. Quick, Jr. and D. S. Moore, J. Chem. Phys. **79**, 759 (1983).
[8]D. P. Gerrity and J. J. Valentini, J. Chem. Phys. **79**, 5202 (1983).
[9]D. P. Gerrity and J. J. Valentini, J. Chem. Phys. **81**, 1298 (1984).
[10]C. T. Rettner, E. E. Marinero, and R. N. Zare, in *Physics of Electronic and Atomic Collisions. Invited Papers from the XVIII ICPEAC, Berlin, July 27–Aug. 2, 1983*, edited by J. Eichler, I. V. Hertel, and N. Stolterfoht (North Holland, Amsterdam, 1984).
[11]E. E. Marinero, C. T. Rettner, and R. N. Zare, J. Chem. Phys. **80**, 4141 (1984).
[12]B. Liu, J. Chem. Phys. **80**, 581 (1984).
[13]D. M. Ceperley and B. J. Alder, J. Chem. Phys. **81**, 5833 (1984).
[14]R. N. Barnett, P. J. Reynolds, and W. A. Lester, Jr., J. Chem. Phys. **82**, 2700 (1985).
[15]D. P. Gerrity and J. J. Valentini, J. Chem. Phys. **82**, 1323 (1985).
[16]D. P. Gerrity and J. J. Valentini, J. Chem. Phys. **83**, 2207 (1985).
[17]J. J. Valentini and D. P. Gerrity, Int. J. Chem. Kinet. **18**, 937 (1986).
[18]H. B. Levene, D. L. Phillips, J.-H. Nieh, D. P. Gerrity, and J. J. Valentini, Chem. Phys. Lett. **143**, 317 (1988).
[19]J.-H. Nieh and J. J. Valentini, Phys. Rev. Lett. **60**, 519 (1988).
[20]D. L. Phillips, H. B. Levene, and J. J. Valentini, J. Chem. Phys. **90**, 1600 (1989).
[21]B. A. Collings, J. C. Polanyi, M. A. Smith, A. Stolow, and A. W. Tarr, Phys. Rev. Lett. **59**, 2251 (1987).
[22]A. Stolow, Ph. D. thesis, University of Toronto, Toronto, Ontario, Canada, 1988.
[23]S. Datz and E. H. Taylor, J. Chem. Phys. **39**, 1986 (1963).
[24]J. Geddes, H. F. Krause, and W. L. Fite, J. Chem. Phys. **56**, 3298 (1972).
[25]G. H. Kwei and V. W. Lo, J. Chem. Phys. **72**, 6265 (1980).
[26]R. Goetting, H. R. Mayne, and J. P. Toennies, J. Chem. Phys. **80**, 2230 (1984).
[27]R. Goetting, H. R. Mayne, and J. P. Toennies, J. Chem. Phys. **85**, 6396 (1986).
[28]R. Goetting, V. Herrero, J. P. Toennies, and M. Vodegel, Chem. Phys. Lett. **137**, 524 (1987).
[29]S. A. Buntin, Ph. D. thesis, University of Minnesota, Minneapolis, Minnesota, 1987.
[30]S. A. Buntin, C. F. Giese, and W. R. Gentry, J. Chem. Phys. **87**, 1443 (1987).
[31]R. E. Continetti, Ph. D. thesis, University of California, Berkeley, California, 1989.
[32]R. E. Continetti, B. A. Balko, and Y. T. Lee (in preparation).
[33]M. Teufel, Diploma thesis, University of Bielefeld, Bielefeld, West Germany, 1987.
[34]I. A. Welge, in *XII International Symposium on Molecular Beams, Abstracts of Invited Talks and Contributed Papers*, May 29–June 2, 1989 (Univ. of Perugia, Perugia, Italy), p. I.10.
[35]F. London, Z. Elektrochem. **35**, 552 (1929).
[36]H. Eyring and M. Polanyi, Z. Phys. Chem. B **12**, 279 (1931).
[37]D. G. Truhlar and R. E. Wyatt, Ann. Rev. Phys. Chem. **27**, 1 (1976).
[38]See Int. J. Chem. Kin. **18**, No. 9 (1986).
[39]G. C. Schatz, in *NATO Research Workshop on the Theory of Chemical Reaction Dynamics* (Cambridge, Cambridgeshire, 1985), *The Theory of Chemical Reaction Dynamics* (Reidel, Boston, 1986).
[40]J. J. Valentini and P. L. Phillips, in *Advances in Gas Phase Photochemistry and Kinetics, Vol. 2. Bimolecular Reactions*, edited by M. N. R. Ashfold and J. F. Baggott (to be published).
[41]P. Siegbahn and B. Liu, J. Chem. Phys. **68**, 2457 (1978).
[42]D. G. Truhlar and C. J. Horowitz, J. Chem. Phys. **68**, 2466 (1978).
[43]D. G. Truhlar and C. J. Horowitz, J. Chem. Phys. **71**, 1514 (1978).
[44]A. C. Varandas, F. B. Brown, C. A. Mead, D. G. Truhlar, and N. C. Blais, J. Chem. Phys. **86**, 6258 (1987).
[45]G. D. Barg, H. R. Mayne, and J. P. Toennies, J. Chem. Phys. **74**, 1017 (1981).
[46]C. A. Booneberg and H. R. Mayne, Chem. Phys. Lett. **108**, 67 (1984).
[47]N. C. Blais and D. G. Truhlar, in *Potential Energy Surfaces and Dynamics Calculations*, edited by D. G. Truhlar (Plenum, New York, 1981).
[48]N. C. Blais and D. G. Truhlar, Chem. Phys. Lett. **102**, 120 (1983).
[49]N. C. Blais, D. G. Truhlar, and B. C. Garrett, J. Chem. Phys. **82**, 2300 (1985).
[50]N. C. Blais and D. G. Truhlar, J. Chem. Phys. **83**, 2201 (1985).
[51]N. C. Blais and D. G. Truhlar, J. Chem. Phys. **88**, 5457 (1988).
[52]G. C. Schatz, Chem Phys. Lett. **108**, 53 (1984).
[53]S. H. Suck Salk, C. R. Klein, and C. K. Lutrus, Chem. Phys. Lett. **110**, 112 (1984); we thank these workers for kindly providing us with their rovibrational populations.
[54]M. S. Bowers, B. H. Choi, R. T. Poe, and K. T. Tang, Chem. Phys. Lett. **116**, 239 (1985).
[55]J. N. L. Connor and W. J. E. Southall, Chem. Phys. Lett. **123**, 139 (1986).
[56]M. C. Colton and G. C. Schatz, Chem. Phys. Lett. **124**, 256 (1986).
[57]C. R. Klein and S. H. Suck Salk, Chem. Phys. Lett. **125**, 481 (1986).
[58]F. Webster and J. C. Light, J. Chem. Phys. **85**, 4744 (1986).
[59]F. Webster and J. C. Light, J. Chem. Phys. **90**, 265, 300 (1989).
[60]A. Kuppermann and P. G. Hipes, J. Chem. Phys. **84**, 5962 (1986).
[61]P. G. Hipes and A. Kuppermann, Chem. Phys. Lett **133**, 1 (1986).
[62]K. Haug, D. W. Schwenke, Y. Shima, D. G. Truhlar, J. Zhang, and D. J. Kouri, J. Phys. Chem. **90**, 6757 (1986).
[63]D. W. Schwenke, K. Haug, D. G. Truhlar, Y. Sun, J. Z. H. Zhang, and D. J. Kouri, J. Phys. Chem. **91**, 6080 (1987).
[64]J. Z. H. Zhang, D. J. Kouri, K. Haug, D. W. Schwenke, Y. Shima, and D. G. Truhlar, J. Chem. Phys. **88**, 2492 (1988).
[65]D. W. Schwenke, K. Haug, M. Zhao, D. G. Truhlar, Y. Sun, J. Z. H. Zhang, and D. J. Kouri, J. Phys. Chem. **92**, 3202 (1988).
[66]B. C. Garrett, D. W. Schwenke, R. T. Skodje, D. Thirumalai, T. C. Thompson, and D. G. Truhlar, in *Resonances in Electron-Molecule Scattering, van der Waals Complexes, and Reactive Chemical Dynamics*, edited by D. G. Truhlar (American Chemical Society Symposium Series No. 263, Washington, 1984), p. 375; M. Mladenovic, M. Zhao, D. G. Truhlar, D. W. Schwenke, Y. Sun, and D. J. Kouri, Chem. Phys. Lett. **146**, 358 (1988); M. Zhao, D. G. Truhlar, D. J. Kouri, Y. Sun, and D. W. Schwenke, *ibid.* **156**, 281 (1989); M. Zhao, M. Mladenovic, D. G. Truhlar, D. W. Schenke, O. Sharafeddin, Y. Sun, and D. J. Kouri, J. Chem. Phys. (in press).

[67]J. Z. H. Zhang and W. H. Miller, J. Chem. Phys. **91**, 1528 (1989).
[68]D. E. Manolopoulos and R. E. Wyatt, Chem. Phys. Lett. **159**, 123 (1989).
[69]R. S. Blake, K.-D. Rinnen, D. A. V. Kliner, and R. N. Zare, Chem. Phys. Lett. **153**, 365 (1988).
[70]K.-D. Rinnen, D. A. V. Kliner, R. S. Blake, and R. N. Zare, Rev. Sci. Instr. **60**, 717 (1989).
[71]D. A. V. Kliner, K.-D. Rinnen, and R. N. Zare, J. Chem. Phys. **90**, 4625 (1989).
[72]D. A. V. Kliner, K.-D. Rinnen, M. A. Buntine and R. N. Zare (unpublished results).
[73]R. S. Mulliken, Phys. Rev. **51**, 310 (1937).
[74]The barium borate crystals were supplied by R. S. Feigelson and R. K. Route and grown as part of a research program sponsored in part by the Army Research Office, Contract No. DAAL03-86-K-0129, and in part by the NSF/MRL Program through the Center for Materials Research, Stanford University.
[75]J. L. Wiza, Nucl. Instrum. Methods **162**, 587 (1979).
[76]R. S. Blake, Ph. D. thesis, Stanford University, Stanford, California, 1988.
[77]P. W. Atkins, *Physical Chemistry* (W. H. Freeman and Company, San Francisco, 1982).
[78]K.-D. Rinnen, D. A. V. Kiner, R. N. Zare, and W. M. Huo, Isr. J. Chem. (in press).
[79]K. -D. Rinnen, D. A. V. Kliner, M. A. Buntine, R. N. Zare, and W. M. Huo (unpublished results).
[80]K.-D. Rinnen, D. A. V. Kliner, R. S. Blake, and R. N. Zare, Chem. Phys. Lett. **153**, 371 (1988).
[81]A. C. Kummel, G. O. Sitz, and R. N. Zare, J. Chem. Phys. **85**, 6874 (1986).
[82]G. N. A. van Veen, K. A. Mohamed, T. Baller, and A. E. de Vries, Chem. Phys. **80**, 113 (1983).
[83]D. K. Veirs, G. M. Rosenblatt, and J. J. Valentini, J. Chem. Phys. **83**, 1605 (1985).
[84]K. P. Huber and G. Herzberg, *Molecular Spectra and Molecular Structure IV. Constants of Diatomic Molecules* (Van Nostrand Reinhold, New York, 1979).
[85]G. W. Johnston, B. Katz, K. Tsukiyama, and R. Bersohn, J. Phys. Chem. **91**, 5445 (1987).
[86]I. Schechter and R. D. Levine, Int. J. Chem. Kinet. **18**, 1023 (1986).
[87]R. D. Levine and R. B. Bernstein, Chem. Phys. Lett. **105**, 467 (1984).
[88]R. D. Levine and R. B. Bernstein, *Molecular Reaction Dynamics and Chemical Reactivity* (Oxford University, New York, 1987).
[89]G. C. Schatz and A. Kuppermann, J. Chem. Phys. **62**, 2504 (1975).
[90]M. J. Redmon and R. E. Wyatt, Int. J. Quantum Chem. Symp. **9**, 403 (1975).
[91]R. E. Wyatt, Chem. Phys. Lett. **34**, 167 (1975).
[92]G. C. Schatz and A. Kuppermann, J. Chem. Phys. **65**, 4642 (1976).
[93]R. B. Bernstein, Int. Quantum Chem. Symp. **10**, 267 (1976).
[94]E. Pollak, Chem. Phys. Lett. **47**, 513 (1977).
[95]E. Zamir, R. D. Levine, and R. B. Bernstein, Chem. Phys. Lett. **107**, 217 (1984).
[96]S. H. Suck Salk, C. K. Lutrus, and D. A. Reago, Jr., Phys. Rev. A **35**, 1074 (1987).
[97]R. D. Levine and J. L. Kinsey, in *Atom–Molecule Collision Theory. A Guide for the Experimentalist*, edited by R. B. Bernstein (Plenum, New York, 1979).
[98]J. C. Light, J. Chem. Phys. **40**, 3221 (1964).
[99]P. Pechukas and J. C. Light, J. Chem. Phys. **42**, 3281 (1965).
[100]P. Pechukas, J. C. Light, and C. Rankin, J. Chem. Phys. **44**, 794 (1966).
[101]N. C. Blais, M. Zhao, M. Mladenovic, D. G. Truhlar, D. W. Schwenke, Y. Sun, and D. J. Kouri, J. Am. Chem. Soc. **111**, 852 (1989).
[102]H. R. Mayne and J. P. Toennies, J. Chem. Phys. **75**, 1794 (1981).
[103]A. A. Westenberg and N. de Haas, J. Chem. Phys. **58**, 1393 (1967).
[104]D. N. Mitchell and D. J. Le Roy, J. Chem. Phys. **58**, 3449 (1973).
[105]N. C. Blais, D. G. Truhlar, and B. C. Garrett, J. Chem. Phys. **78**, 2363 (1983).
[106]D. M. Garner, D. G. Fleming, and R. J. Mikula, Chem. Phys. Lett. **121**, 80 (1985).
[107]I. D. Reid, D.M. Garner, L. Y. Lee, M. Senba, D. J. Arseneau, and D. G. Fleming, J. Chem. Phys. **86**, 5578 (1987).
[108]N. C. Blais and D. G. Truhlar, Chem. Phys. Lett. (to be published).
[109]G. C. Schatz, Annu. Rev. Phys. Chem. **39**, 317 (1988).
[110]N. C. Blais and D. G. Truhlar, J. Chem. Phys. **65**, 5335 (1976).
[111]D. G. Truhlar, B. P. Reid, D. E. Zurawski, and J. C. Gray, J. Phys. Chem. **85**, 786 (1981).
[112]G. C. Schatz (private communication).